IOPscience iopscience.iop.org

Home Search Collections Journals About Contact us My IOPscience

Terahertz oscillations in ultra-thin n-$In_{0.53}Ga_{0.47}As$ ungated channels

This article has been downloaded from IOPscience. Please scroll down to see the full text article.

2008 J. Phys.: Condens. Matter 20 384210

(http://iopscience.iop.org/0953-8984/20/38/384210)

View the table of contents for this issue, or go to the journal homepage for more

Download details:
IP Address: 129.252.86.83
The article was downloaded on 29/05/2010 at 15:07

Please note that terms and conditions apply.

J. Phys.: Condens. Matter **20** (2008) 384210 (7pp) doi:10.1088/0953-8984/20/38/384210

Terahertz oscillations in ultra-thin n-$In_{0.53}Ga_{0.47}As$ ungated channels

J-F Millithaler[1], L Reggiani[1], J Pousset[2], G Sabatini[2], L Varani[2], C Palermo[2], J Mateos[3], T González[3], S Perez[3] and D Pardo[3]

[1] Dipartimento di Ingegneria dell'Innovazione and CNISM, Università del Salento, Via Arnesano s/n, 73100 Lecce, Italy
[2] Institut d'Électronique du Sud, UMR CNRS 5214, Université Montpellier II, Place Bataillon, 34095 Montpellier Cedex 5, France
[3] Departamento de Fisicà Aplicada, Universidad de Salamanca, Pza. Merced s/n 37008 Salamanca, Spain

E-mail: jf.millithaler@unile.it

Received 28 March 2008, in final form 24 April 2008
Published 21 August 2008
Online at stacks.iop.org/JPhysCM/20/384210

Abstract
Using a self-consistent Monte Carlo simulator we investigate the spectrum of voltage fluctuations of an n-type InGaAs two-terminal layer of variable thickness W in the range 1–100 nm and variable length L in the range 0.01–10 μm embedded in an external dielectric medium. Calculations are performed at $T = 300$ K for different dopings and in the presence of an external bias of increasing strength. When the bias is well below the threshold for the Gunn effect the spectrum peaks at the plasma oscillations of the electron gas. For $W \geqslant 100$ nm and carrier concentrations of 10^{17}–10^{18} cm^{-3} the peaks are in good agreement with the standard three-dimensional (3D) expression of the plasma frequency. For $W \leqslant 10$ nm the results exhibit a plasma frequency that depends on the length of the layer, thus implying that the oscillation mode is dispersive. The corresponding frequency covers a wide range of values 0.1–10 THz and is in agreement with the two-dimensional (2D) expression of the plasma frequency obtained for a collisionless regime within the in-plane approximation for the electric field. A region of cross-over between the 2D and 3D behaviours of the plasma frequency is shown for $W > 10$ nm. When the bias is above the threshold for the Gunn effect, we observe the washing out of the plasma peak and the onset of a frequency peak associated with the transit time of the Gunn domain located in the sub-terahertz frequency region.

1. Introduction

Generation and/or detection of electromagnetic radiation in the terahertz (THz) domain is a subject that is developing quickly because of its potential applications in different branches of advanced technologies, such as broadband communications, high-resolution spectroscopy, environment monitoring, biomedical testing, etc [1, 2]. As a consequence, the realization of solid-state devices operating in the THz domain at room-temperature and with compact, powerful, and tunable characteristics is a mandatory issue. To this purpose, one of the most promising strategies lies in the plasmonic approach. In this framework, through an analytical approach, the case of a two-dimensional (2D) electron layer constituted by the ungated channel of a nanometric transistor was considered in [3, 4]. The electron gas was assumed to be highly concentrated but nondegenerate, and supposed to undergo only long-range electron–electron interaction. By making a small signal analysis of the self-consistent set of coupled equations consisting of kinetic and Poisson equations, the last within the in-plane field approximation, the electron gas was found to behave as the support of plasma waves whose propagation velocity can be greater than the electron drift velocity. The frequency value of these plasma waves, besides the intrinsic parameters of the material, such as carrier concentration and carrier effective mass, was found to be controlled by the geometry of the structure as well as by the external dielectric which surrounds the semiconductor layer. Through the oscillations of the plasma, nanometric high electron mobility transistors (HEMT) have been suggested as

 © 2008 IOP Publishing Ltd Printed in the UK

possible emitters and detectors of electromagnetic radiation in the terahertz range [5].

The aim of this work is to investigate the same problem from a microscopic point of view, thus testing the limits of applicability of the analytical approach and exploiting possible implementations. To this purpose, we consider an n-type $In_{0.53}Ga_{0.47}As$ layer, embedded in a symmetric dielectric, in the presence of an external bias of arbitrary strength and analyse the frequency spectrum of voltage fluctuations obtained from a Monte Carlo simulator coupled with a 2D Poisson solver. The cases of the ohmic regime and current saturation regime are both considered. In the former regime, the spectrum is characterized by a peak at the plasma frequency associated with the carrier oscillations due to the self-consistent electric field [6]. In the latter regime, because of the presence of negative differential mobility (NDM) conditions, the spectrum is characterized by the onset of a peak which is the precursor of the establishment of current oscillations due to periodic travelling of the Gunn domains associated with the presence of NDM [7]. Because of the material parameters and the considered geometries, the frequencies associated with the peaks of the voltage spectral density span a wide range of values centred in the terahertz region.

The content of the work is organized as follows. Section 2 presents the theoretical approaches underlying the present investigation. Section 3 reports and discusses the numerical results obtained by a self-consistent Monte Carlo simulator. Major conclusions are summarized in section 4.

2. Theory

In this section we briefly survey the analytical approach and the Monte Carlo simulator applied to the device under test.

2.1. Analytical model

The analytical model considers a 2D sheet of electrons in the $\vec{r} \equiv xy$-plane embedded in a dielectric along the z direction. Carriers move under collisionless conditions in the presence of self-consistent in-plane electric field $\mathbf{E} = -\nabla U$, with U the electrical potential described by the Poisson equation:

$$\nabla^2 U(\mathbf{r}, z, t) = \frac{e n^{2\mathrm{D}}(\mathbf{r}, t)}{\varepsilon_0 \varepsilon_{\mathrm{diel}}} \delta(z) \quad (1)$$

with e the electron charge, $n^{2\mathrm{D}}$ the local 2D carrier concentration, $\varepsilon_{\mathrm{diel}}$ the relative dielectric constant of the outside dielectric, and ε_0 the vacuum permittivity. Within a small signal analysis, the corresponding wave equation for the Fourier transform of $n^{2\mathrm{D}}$, $n_k^{2\mathrm{D}}$ leads to a dispersive 2D plasma frequency

$$f_{\mathrm{p}}^{2\mathrm{D}} = \frac{1}{2\pi} \sqrt{\frac{e^2 n_0^{2\mathrm{D}} |\mathbf{k}|}{2 m_0 m \varepsilon_0 \varepsilon_{\mathrm{diel}}}} \quad (2)$$

where $|\mathbf{k}|$ is the modulus of the wavevector in the k_x, k_y plane, m_0 and m the free and effective electron masses, respectively, and $n_0^{2\mathrm{D}}$ the average 2D carrier concentration. We notice that the 2D plasma frequency depends on the relative dielectric constant of the external dielectric.

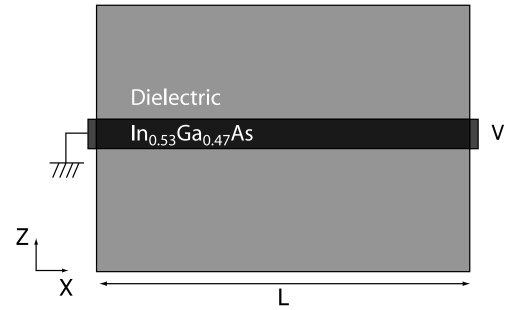

Figure 1. Schematic diagram of the device (not to scale) studied within the Monte Carlo simulation. The free charge is present only in the bar of length L along the x direction and thickness W along the z direction. The terminal at the left-hand side is the source contact kept at a voltage $V = 0$ the terminal at the right-hand side is the drain contact kept at a potential V. Carriers are reflected at the boundaries between the bar and the dielectric.

Plasma waves also exist in bulk and their three-dimensional (3D) dispersionless frequency is

$$f_{\mathrm{p}}^{3\mathrm{D}} = \frac{1}{2\pi} \sqrt{\frac{e^2 n_0^{3\mathrm{D}}}{m_0 m \varepsilon_0 \varepsilon_{\mathrm{mat}}}} \quad (3)$$

with $n_0^{3\mathrm{D}}$ the 3D average carrier concentration and $\varepsilon_{\mathrm{mat}}$ the relative dielectric constant of the bulk material.

2.2. Monte Carlo simulations

The numerical solution of this problem is carried out by using a microscopic Monte Carlo approach coupled with a 2D Poisson solver [5, 8]. By evaluating the fluctuations of the voltage around the steady value in the centre of the device under test, the spectral density of this quantity is obtained from the corresponding correlation function, and the characteristic peaks exhibited by the spectrum before cut-off are analysed as detailed in [6]. To study the proper oscillations of the electron gas, we simulate a bar of $In_{0.53}Ga_{0.47}As$ of length L in the range 0.01–10 μm for different thicknesses W in the range 1–100 nm, and carrier concentrations of 10^{17} and 10^{18} cm^{-3}, with the two terminals of the bar connected by ideal ohmic contacts. The contacts are realized by an infinite reservoir of thermalized electrons at electrochemical potentials differing by eU with U the applied voltage [9]. The bar is surrounded by a perfect dielectric (here taken as the vacuum) 10 μm wide in the upper and lower region of the bar, where the 2D Poisson equation in the xz-plane is solved to account for the fringing of the external electric field. The third dimension is used to relate the number of simulated carriers with the 3D carrier concentration. For a comparative analysis between numerical simulations and analytical results we take $k = 2\pi/L$ and $n_0^{2\mathrm{D}} = n_0^{3\mathrm{D}} \cdot W$. The simulated structure, which is depicted in figure 1, represents a simplified version of an ungated transistor channel. The time and space discretizations take typical values of 0.2–1 fs for the time step, 0.1–5 nm for the spatial scale of the bar and 500 nm for the spatial scale of the dielectric. Typically there are about 80 carriers inside a mesh of the bar, which are found to provide a reliable solution of the Poisson

Table 1. Parameters of $In_{0.53}Ga_{0.47}As$.

Parameters	$In_{0.53}Ga_{0.47}As$		
Density (kg m^{-3})	5.545		
Sound velocity (m s^{-1})	4.756		
Static dielectric constant	13.88		
Optical dielectric constant	11.35		
LO phonon energy (eV)	0.0328		
Energy gap (eV)	0.7		
Alloy scattering potential (eV)	1.50		
	Γ	L	X
Effective mass (m^*/m_0)	0.042	0.258	0.538
Nonparabolicity (eV^{-1})	1.255	0.461	0.204
Energy level from Γ (eV)	0.0	0.61	1.11
Number of equivalent valleys	1	4	3
Acoustic deformation potential (eV)	5.887	10.84	9.657
Optical deformation potential (10^{10} eV m^{-1})	0.0	3.79	0.0
Optical phonon energy (eV)	0.0	0.0369	0.0
Intervalley deformation potential (10^{10} eV m^{-1})			
From Γ	0.0	7.827	11.32
From L	7.827	6.40	6.80
From X	11.32	6.80	8.537
Intervalley phonon energy (eV)			
From Γ	0.0	0.025 42	0.025 79
From L	0.025 42	0.2481	0.030 21
From X	0.025 79	0.030 21	0.028 41

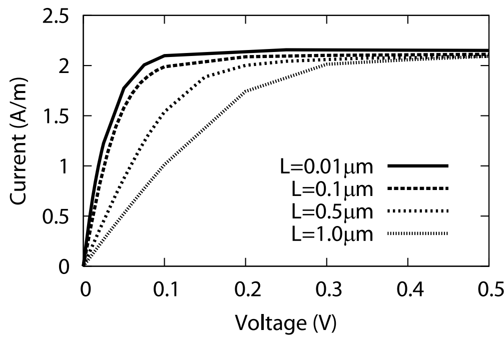

Figure 2. Current–voltage characteristics for a density of $n_0^{3D} = 10^{17}$ cm^{-3}, $W = 1$ nm and for different lengths. The current is given in A m^{-1} units because the third dimension does not enter the Poisson solver, and serves only to convert the number of simulated carriers into the 3D carrier concentration.

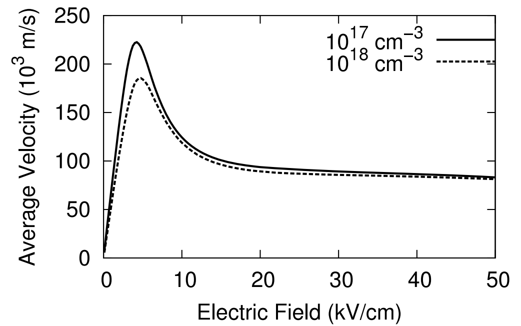

Figure 3. Velocity-field characteristic for a bulk $In_{0.53}Ga_{0.47}As$ with $n_0^{3D} = 10^{17}$ and 10^{18} cm^{-3}, respectively at $T = 300$ K.

equation. Table 1 reports the microscopic parameters of the material considered in the calculations.

3. Results and discussion

Figure 2 reports the current–voltage characteristics for typical lengths in the range 0.01–1 μm and $n_0^{3D} = 10^{17}$ cm^{-3}. The curves exhibit a linear (ohmic) regime at the lowest voltages and a saturation regime at the highest voltages, as expected for such a structure. For length $L \leqslant 0.1$ μm the transport enters the ballistic regime and the resistance is found to become independent of the length according to the ballistic expression [10]

$$R^{\text{bal}} = \frac{2}{Ae^2 n_0^{3D}} \sqrt{\frac{2k_B T m m_0}{\pi}} \quad (4)$$

with A the cross-sectional area.

Figure 3 reports the velocity-field characteristics of the bulk material with the electric field taking values covering the range of the corresponding values of the voltage in figure 2. Here, the peak velocity associated with the Gunn effect is found to be 2.2×10^7 cm s^{-1} at the threshold field of 4.2 kV cm^{-1} for $n = 10^{17}$ cm^{-3} and 1.9×10^7 cm s^{-1} at the threshold field of 4.7 kV cm^{-1} for $n = 10^{18}$ cm^{-3}, respectively.

In the following, we investigate the spectrum of voltage fluctuations in the frequency range 0.01–100 THz where peaks associated with plasma oscillations and/or current oscillations due to Gunn domains are expected depending on the strength of the applied voltage.

3.1. Ohmic regime

Figure 4 reports a typical spectrum of voltage fluctuations normalized to its zero frequency value for the case of $L = 0.1$ μm, $W = 100$ nm, $n_0^{3D} = 10^{17}$ cm^{-3} in the absence of an

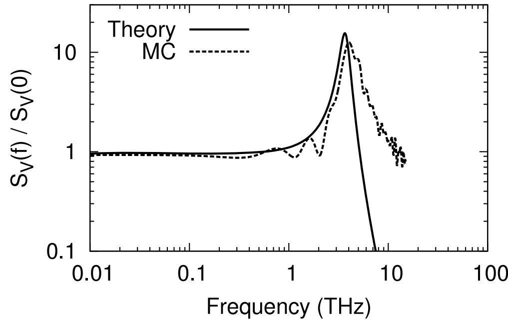

Figure 4. Spectral density of voltage fluctuations normalized to the static value in an $In_{0.53}Ga_{0.47}As$ channel of length $L = 0.1$ μm, width $W = 1$ nm at thermodynamic equilibrium. The dashed curve refers to simulations and the continuous curve to the theoretical expression of the equivalent circuit.

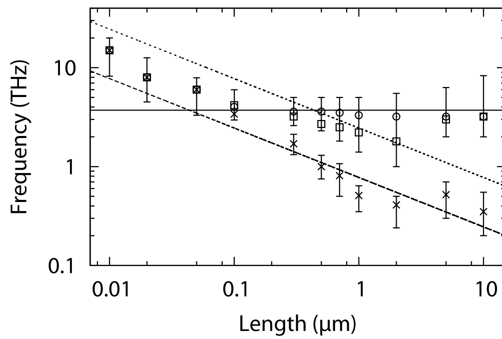

Figure 5. Frequency peak of the voltage spectral density at thermodynamic equilibrium as a function of the channel length for $n_0^{3D} = 10^{17}$ cm^{-3} and different channel widths $W = 1$, 10, and 100 nm, shown by crosses, open squares, open circles, respectively. Error bars give the full width at half the peak shape. The straight line refers to the theoretical 3D plasma frequency, the dashed and dotted line to the theoretical 2D plasma frequencies for $W = 1$ nm and $W = 10$ nm, respectively.

applied voltage. The results of the simulation (dotted curve) are compared with those obtained by the 3D impedance equivalent circuit (continuous curve) [11]:

$$\frac{S_V(f)}{S_V(0)} = \frac{1}{[1 - (2\pi f \tau_P)^2]^2 + (2\pi f \tau_d)^2} \qquad (5)$$

with f the frequency, $\tau_P = 4.28 \times 10^{-14}$ s, and $\tau_d = 1.07 \times 10^{-14}$ s the plasma and dielectric relaxation times corresponding to the simulated bulk material. Here, the plasma peak is well evidenced by the good qualitative fit between numerical and theoretical results. We notice that simulations evidence a cut-off decay as f^{-2}, which is reminiscent of the presence of scattering mechanisms. Indeed, the f^{-2} shoulder exhibited by MC simulations intercepts the f^{-4} decay at about 5 THz which is the collision rate associated with the electron mobility. The analogous investigation for the case of $n_0^{3D} = 10^{18}$ cm^{-3} gives a collision rate of about 12 THz owing to the higher efficiency of ionized impurity scattering over intravalley phonon scattering whose scattering rate is estimated to be about 3 THz. In the ohmic regime, intervalley scattering is negligible and only the central valley is populated.

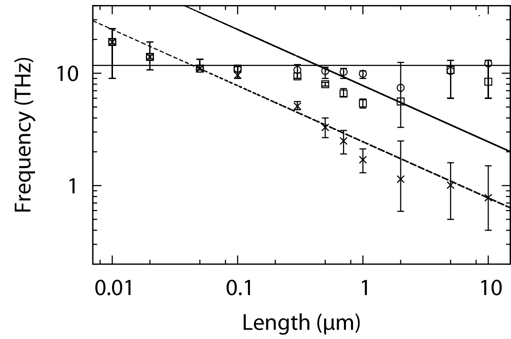

Figure 6. Frequency peak of the voltage spectral density at thermodynamic equilibrium as a function of the channel length for $n_0^{3D} = 10^{18}$ cm^{-3} and different channel widths $W = 1$, 10, and 100 nm, shown by crosses, open squares, and open circles, respectively. Error bars give the full width at half the peak shape. The straight line is the theoretical 3D plasma frequency and the dashed and dotted lines are the theoretical 2D plasma frequencies for $W = 1$ nm and $W = 10$ nm, respectively.

Figure 5 reports the frequency of the peak exhibited by the spectral density of voltage fluctuations as a function of the channel length for different widths of the channel and a carrier concentration of 10^{17} cm^{-3}. Here, the error bars give the full width at half the peak thus providing the broadening of the shape peak. Since the carrier mean free path is about 100 nm, for lengths above about 100 nm the transport regime is diffusive and the peak before cut-off is attributed to the plasma frequency of the electron gas. For lengths below about 100 nm the transport enters the ballistic regime and the values of the frequency peak above the 3D plasma values might be attributed to the mixed action of 2D plasma oscillations and ballistic transport. In the diffusive regime we found: (i) for $W = 1$ nm a reasonable agreement of the frequency peak with the 2D analytical formula in equation (2) in the whole range of lengths (here, by exploiting the predictivity of the analytical results quantum effects are disregarded); (ii) for $W = 100$ nm, the frequency peak well agrees with the 3D analytical formula in equation (3) in the whole range of lengths; (iii) for $W = 10$ nm, a reasonable agreement of the frequency peak with the 2D analytical formula in equation (2) is limited to channel lengths in the 0.1–2 μm range, indeed, for L greater than 2 μm the frequency peak recovers the value of the 3D case, as for $W = 100$ nm.

Figure 6 reports the analogous results of figure 5 for a carrier concentration of 10^{18} cm^{-3}. Apart for the blue shift of the plasma frequency, due to the increased carrier concentration, we have found a behaviour which parallels that of figure 5. Even here, ballistic effects appear for lengths shorter than 100 nm and they are of less importance with respect to those of the previous case.

We conclude that the simulations provide evidence for the presence of a cross-over between the 2D and 3D behaviour of the plasma frequency, not predicted by the analytical approach [3], which is controlled by the thickness and/or the length of the channel. The frequency peak covering different cases is in the 0.2–20 THz region.

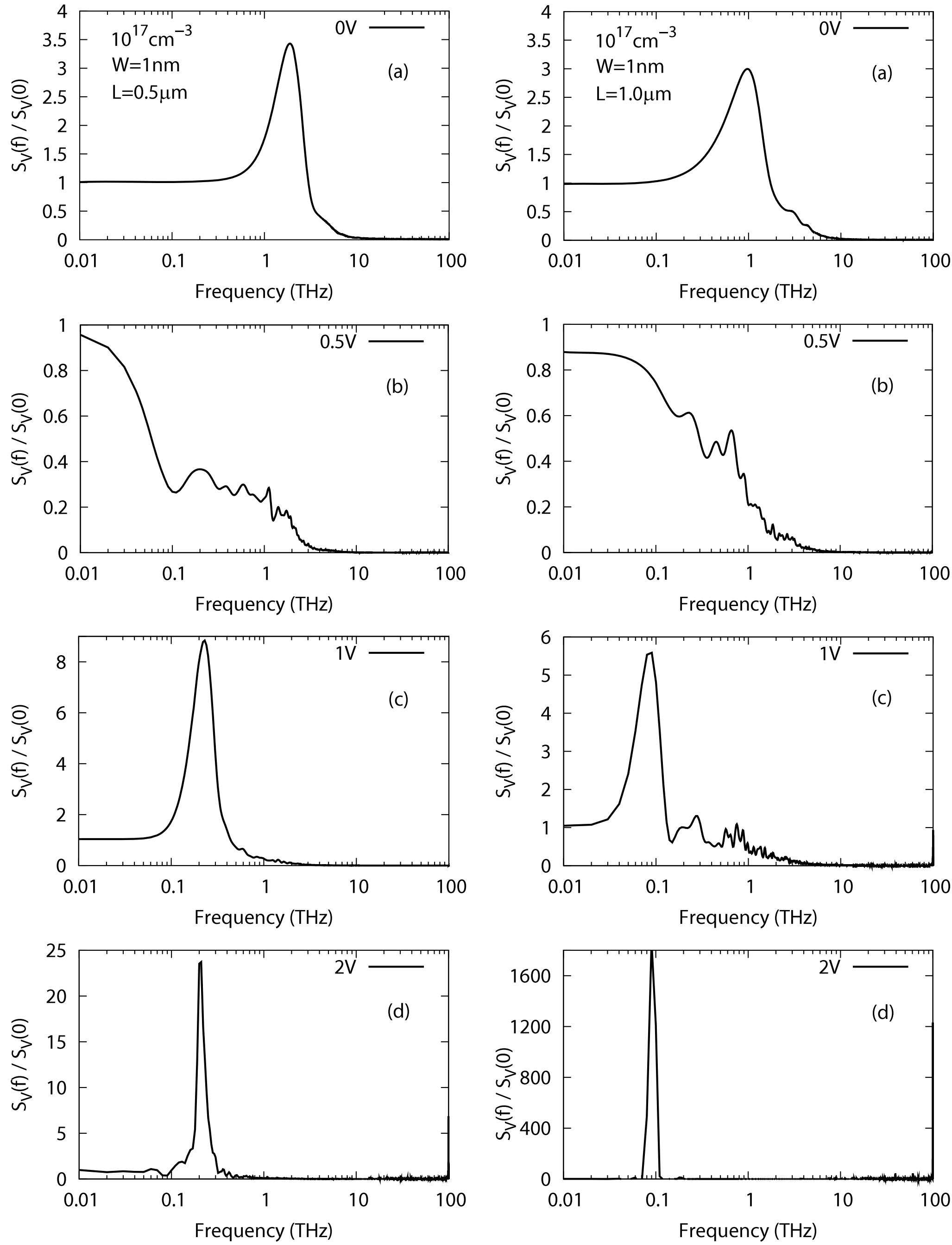

Figure 7. Spectrum of voltage fluctuations normalized to the static value for $L = 0.5$ and $1.0\ \mu$m (left and right columns, respectively), with $W = 1$ nm, $n_0^{3D} = 10^{17}$ cm^{-3}, and applied voltages in the range 0–2 V.

3.2. Saturation regime

Figure 7 reports the spectral density of voltage fluctuations for $L = 0.5\ \mu$m, left column, and $L = 1\ \mu$m, right column, with $n_0^{3D} = 10^{17}$ cm^{-3}, $W = 1$ nm, and at increasing voltages up to 2 V corresponding to velocity-field characteristics entering inside the NDM region. Here, the presence of NDM starts playing a dominant role at 0.5 V, see figure 7(b), where the plasma peak clearly seen at 0 V is replaced by a shoulder region in the range 0.1–2 THz, just before cut-off. Then, by further increasing the voltage at 1 V, see figure 7(c), we observe the onset of a frequency peak in the range of 0.1–0.2 THz, which is a precursor for the onset of current oscillations due to travelling Gunn domains. Current oscillations have been observed in simulations at $U = 2$ V for channel lengths above about 1 μm (see figure 7 (d) right column), where the Kroemer criterion [12] $n_0^{3D}L > 10^{11}$ cm^{-2} is satisfied. This interpretation is confirmed by the fact that the frequency peak shifts at lower frequencies, as the length of the channel increases, with a $1/L$ behaviour as expected. We notice that at around 1 V the population of higher valleys becomes of increasing importance and dominates above about 2 V.

Figure 8 reports the analogous results of figure 7 for the case of $n_0^{3D} = 10^{18}$ cm^{-3}. As expected, when compared to

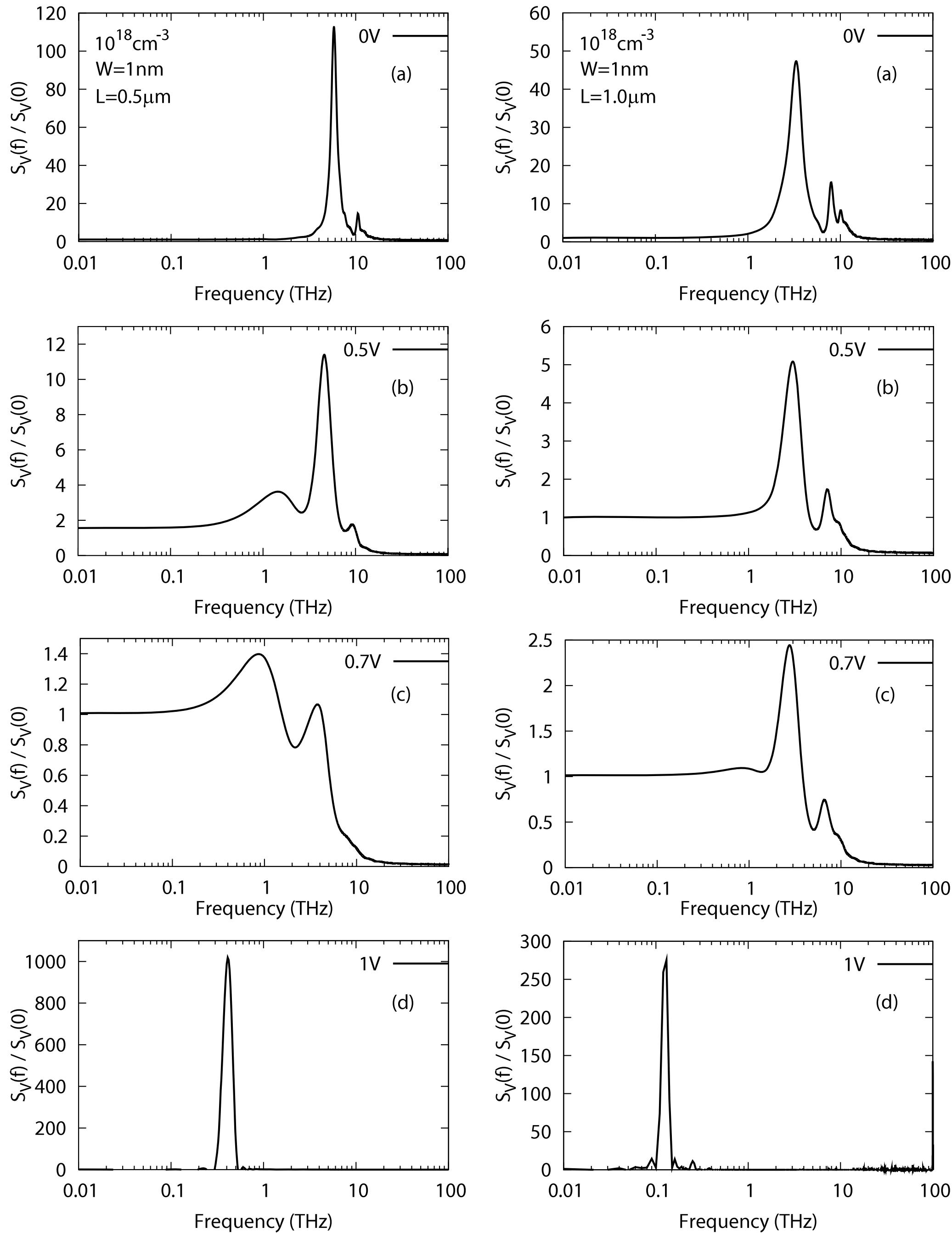

Figure 8. Spectrum of voltage fluctuations normalized to the static value for $L = 0.5$ and 1.0 μm (left and right columns, respectively), with $W = 1$ nm, $n_0^{3D} = 10^{18}$ cm^{-3}, and applied voltages in the range 0–1 V.

the previous case of $n_0^{3D} = 10^{17}$ cm^{-3}, the increased carrier concentration is found to enhance the height of the plasma peaks and of those associated with the Gunn oscillations. Here, the plasma peak is replaced by that associated with Gunn oscillations above about 0.7 V (see figure 8(c)) and the onset of current oscillations is found already at 1 V for both the considered lengths (see figure 8(d)).

We conclude that by increasing the applied voltage to values inside the NDM region, the plasma peak is washed out in favour of the appearance of a new peak, which is a precursor of the onset of current oscillations due to the establishment of the Gunn domains. For the considered channel lengths, the values of these Gunn oscillations are found to be in the range 0.1–0.5 THz.

4. Conclusions

Through a Monte Carlo calculation of the spectral density of voltage fluctuations we have investigated THz oscillations in $In_{0.53}Ga_{0.47}As$ channels embedded in an external dielectric as a function of channel length and thickness, carrier concentration, and strength of the applied voltage. The microscopic investigation of the characteristic frequency peaks in voltage fluctuations of ultra-thin InGaAs channels provide evidence for

a rich scenario, only partially predicted by the 2D collisionless analytical model [3].

Under near thermal equilibrium (ohmic) conditions, the results of simulations show that for thick channels, i.e. W above 100 nm, 3D plasma oscillations appear independently of the channel length in the presence of the diffusive transport regime. By contrast, for thin channels, i.e. W below 100 nm, we have observed the transition from 3D to 2D plasma modes where the plasma frequency decreases with increasing the length of the channel, in good agreement with the analytical model [3]. The simulations show: (i) that the presence of scattering does not influence the value of the plasma frequency predicted by the collisionless theory and (ii) the existence of a cross-over between the 2D and 3D behaviour of the plasma frequency, which happens at thicknesses above about 10 nm. In these conditions the frequency peak can take values in a wide range of frequencies from 0.2 to 10 THz according to different channel geometries and carrier concentrations.

Under saturation conditions, the results of simulations show: (i) the onset of a frequency peak, associated with the presence of NDM conditions, (ii) the onset of current oscillations, due to the transit of Gunn domains, and (iii) the washing out of the plasma peak. In this case the value of the frequency peak scales with the inverse of the channel length, taking values in a somewhat narrow frequency range 0.1–0.5 THz for channel lengths in the region 0.2–1 μm.

Acknowledgments

The work was supported by: CNRS-GDR and GDR-E projects ‘Semiconductor sources and detectors of THz frequencies’, the Region Languedoc-Roussillon project ‘Platforme Technologique THz’, the Dirección General de Investigación (MEC, Spain), the FEDER through the project TEC2007-61259MIC and the Action integrada HF 2007-0014, the Italy–France bilateral project Galileo 2007-2008, and the Spain–France bilateral project Picasso 2007-2008.

References

[1] Mittleman D, Gupta M, Neelamani R, Baraniuk J, Rudd R and Koch M 1999 *Appl. Phys.* B **68** 1085
[2] Wollard D L, Brown E R, Pepper M and Kemp M 2005 *Proc. IEEE* **93** 1722
[3] Dyakonov M and Shur M S 2005 *Appl. Phys. Lett.* **87** 111501
[4] Dyakonov M and Shur M 2001 *TeraHertz Sources and Systems* (*NATO Science Series, II. Mathematics, Physics and Chemistry* vol 27) ed M E Miles (Boston, MA: Kluwer Academic) pp 187–207
[5] Lusakowski J, Knap W, Dyakonova N, Varani L, Mateos J, González T, Roelens Y, Bollaert S, Cappy A and Karpierz K 2005 *J. Appl. Phys.* **97** 064307
[6] Millithaler J-F, Reggiani L, Pousset J, Varani L, Palermo C, Knap W, Mateos J, González T, Perez S and Pardo D 2008 *Appl. Phys. Lett.* **92** 042113
[7] Shiktorov P, Gruzhinskis V, Starikov E, Reggiani L and Varani L 1996 *Phys. Rev.* B **54** 8821
[8] Mateos J, González T, Pardo D, Hoël V and Cappy A 2000 *IEEE Trans. Electron Devices* **47** 1950
[9] Bulashenko O M, Mateos J, Pardo D, Gonzalez T, Reggiani L and Rubi J M 1998 *Phys. Rev.* B **57** 1366
[10] Greiner A, Reggiani L, Kuhn T and Varani L 2000 *Semicond. Sci. Technol.* **15** 1071
[11] Varani L and Reggiani L 1994 *Riv. Nuovo Cimento* **17** 1
[12] Kroemer H 1964 *Proc. IEEE* **52** 1736